Journal of Catalysis 259 (2008) 250–259

Contents lists available at ScienceDirect

Journal of Catalysis

www.elsevier.com/locate/jcat

Effect of support materials on Ag catalysts used for acrylonitrile decomposition

Tetsuya Nanba *, Shouichi Masukawa, Junko Uchisawa, Akira Obuchi

National Institute of Advanced Industrial Science and Technology (AIST), Research Center for New Fuels and Vehicle Technology, 16-1 Onogawa, Tsukuba 305-8569, Japan

ARTICLE INFO

Article history:
Received 17 May 2008
Revised 25 August 2008
Accepted 26 August 2008

Keywords:
Acrylonitrile
Decomposition
Silver

ABSTRACT

The effect of the support material on the Ag-catalyzed decomposition of acrylonitrile (AN) to form N_2 was studied for catalyst systems of Ag-ZSM-5, Ag/Al_2O_3, Ag/TiO_2, Ag/SiO_2, Ag/MgO, and Ag/ZrO_2. Ag/TiO_2 and Ag/SiO_2 exhibited high AN conversion with high N_2 selectivity. X-ray diffraction, ultraviolet–visible spectroscopy, and H_2 temperature-programmed reduction revealed that both metallic and oxidized Ag species were present on TiO_2 and SiO_2. On the basis of diffuse reflectance infrared Fourier transform spectroscopy measurements, NH_3 appeared to be formed by hydrolysis of AN, and this hydrolysis was enhanced by the presence of oxidized Ag species in the catalysts. The high AN decomposition activity was due to the presence of both oxidized and metallic Ag species, which promoted the hydrolysis of AN to form NH_3 and the subsequent oxidation of NH_3 to N_2, respectively.

1. Introduction

Emission control of volatile organic compounds (VOCs) is important, because many VOCs have hazardous properties [1]. Incineration is a simple way to remove VOCs, but the process is normally operated at high temperatures, around 800 °C [2]. Catalytic oxidation can decrease the operation temperature for incineration, and such catalytic removal has been studied extensively [3]. Recently, combinations of catalysts with ozone and plasma also have been studied as a means to further decrease incineration temperatures [4,5].

VOCs include many nitrogen-containing compounds. The presence of these nitrogen atoms causes the formation of harmful byproducts during incineration; for example, incineration and catalytic oxidation cause the formation of nitrogen oxides (NO_x) [2,6]. Some catalytic treatments generate other nitrogen-containing compounds, such as HCN [7]; therefore, the conversion of nitrogen in VOCs to inert products, such as N_2, is highly desirable.

In this report, we focus on the catalytic removal of acrylonitrile ($CH_2{=}CH{-}C{\equiv}N$; referred to herein as AN), because AN is known to be a carcinogenic VOC [8]. AN is a raw material of resins, such as acrylonitrile–butadiene–styrene and acrylonitrile–styrene, and a raw material for the synthesis of chemicals, such as acrylic acid or acrylamide. AN has a vapor pressure of 23.1 Torr at 0 °C, and its half-life in the atmosphere is estimated to be 2–3 days. These values are greater than those of benzene, which is also known to be carcinogenic [9]. The threshold limit of AN in work environments is as low as 2 ppm in the United States and Japan. Furthermore, AN is specified in Japan as one of 22 kinds of harmful pollutants for which primary efforts to prevent release into the atmosphere should be made. Therefore, the development of both a treatment system for local exhaust gas containing AN and a method for controlling AN concentrations in working environments is very important.

The complete oxidation of AN over noble metal catalysts has been reported, but no evaluation of the formation of N_2 was carried out in these studies [10]. We previously explored catalysts that successfully convert AN into CO_2, H_2O, and N_2 rather than NO_x [6]. Ag is an efficient catalyst for AN decomposition [6]. Although Al_2O_3 is generally an effective Ag support for environmental catalysis applications, such as nitrogen oxide abatement and catalytic oxidations [11–16], TiO_2, SiO_2, and ZrO_2 are more effective supports for AN decomposition [6]. In this study, we investigated Ag catalysts supported on various materials to clarify the relationship between the AN decomposition activity and the oxidation state of Ag, as well as the role of the support material in promoting catalytic activity.

2. Experimental

2.1. Catalyst preparation

Silver catalysts supported on five kinds of metal oxide were prepared by incipient wetness impregnation. $AgNO_3$ (Wako Pure Chemical Industries) was used for the Ag precursor. The following metal oxides were used as support materials: Al_2O_3 (KHS-46; Sumitomo Chemical), SiO_2 (Wakogel C-100; Wako Pure Chemical Industries), TiO_2 (P-25; Nippon-Aerosil), ZrO_2 (RSC-H; Daiichi-Kigenso), and MgO (Nacalai Tesque). The amount of Ag loaded on the supports was adjusted to 5 wt% for each sample.

* Corresponding author. Fax: +81 29 861 8259.
E-mail address: tty-namba@aist.go.jp (T. Nanba).

0021-9517/$ – see front matter
doi:10.1016/j.jcat.2008.08.013

Ag supported on ZSM-5 was prepared by ion exchange of NH_4-ZSM-5, which was prepared by ion exchange of Na-ZSM-5 (HSZ-820NAA, SiO_2/A_2O_3 molar ratio = 23.8; Tosoh) with aqueous 1 mol/L NH_4NO_3. The Ag loading was 7.4 wt%, as measured by inductively coupled plasma emission spectroscopy (Seiko Electronics; SPS 1200A).

After impregnation or ion exchange, the samples were dried at 110 °C for 12 h and then calcined at 500 °C in static air for 4 h at a ramp rate of 10 °C/min. After calcination, the catalysts were pelletized and sieved to yield granules ranging in with size from 250 to 600 μm.

2.2. Activity tests

A fixed-bed flow reactor system operated at atmospheric pressure was used to test the activity of the catalysts. Each catalyst (0.1 g) was placed in a quartz tube, and the reactant gas was flowed through the tube at a flow rate of 160 ml/min. The reactant gas was composed of He containing approximately 200 ppm AN and 5% O_2. AN vapor was produced by passing He at a predetermined flow rate through liquid AN maintained at −18 °C. Before activity measurement, the sample was pretreated by heating to 500 °C under 5% O_2 at a ramp rate of 20 °C/min and then maintaining this temperature for 1 h. The catalytic activity was measured for steady-state reactions at temperatures from 500 to 200 °C in step of 25 °C. Gas chromatography (GC) and Fourier transform infrared spectroscopy (FT-IR) were used to analyze the catalysis products. The gas chromatograph (Agilent; M200) was equipped with an MS-5A PLOT column (for H_2, N_2, CH_4, and CO analysis) and a PoraPLOT Q column (for CO_2, N_2O, and C_2–C_3 hydrocarbon analysis), as well as a thermal conductivity detector (TCD) for each column. An FT-IR spectrometer (Nicolet; Magna 560), equipped with a multi-reflection gas cell (Gemini Specialty Optics Mercury series; optical path length = 2 m) and a mercury–cadmium–telluride detector, was used for analysis of gaseous NO, NO_2, AN, and other nitrogen-containing products. FT-IR measurements were performed with a resolution of 0.5 cm^{-1}, and each spectrum was obtained by integration of 50 scans. The validity of product analysis was within 10 ppm [17]. Catalytic activity was evaluated in terms of AN conversion and product selectivity:

$$\text{AN conversion (\%)} = \frac{\text{Inlet AN (ppm)} - \text{Outlet AN (ppm)}}{\text{Inlet AN (ppm)}} \times 100,$$

$$\text{Product selectivity (\%)} = \frac{\text{N in product of interest (ppm)}}{\text{Total product N (ppm)}} \times 100.$$

To ensure reliability, the selectivities were evaluated only for AN conversion >5%.

Temperature-programmed surface reactions (TPSR) of the adsorbed AN were carried out in the same apparatus used for the activity tests. Each sample was pretreated in 5% O_2/He at 500 °C for 2 h (oxidizing conditions) or in 5% H_2/He at 400 °C for 1 h (reducing conditions). After pretreatment, the samples were cooled to 50 °C in He, and the reactant gas was flowed for 1 h over the samples at a rate of 160 ml/min, allowing AN to adsorb on the samples. The samples then were heated to 500 °C at a rate of 5 °C/min in 1% O_2/He at a flow rate of 160 ml/min.

The species present on the surface of the catalysts under the conditions used for TPSR were observed by in situ diffuse reflectance infrared Fourier transform spectroscopy (DRIFTS), using a Nicolet Nexus 870. Each sample was pretreated under oxidizing or reducing conditions as described above, and a background spectrum was obtained at room temperature in a 1% O_2/He flow. AN was then adsorbed on the sample from the flowing reactant gas at room temperature. After the sample was purged in He for 20 min, the temperature was raised at a rate of 10 °C/min in a 1% O_2/He flow. After the temperature reached a predetermined point, the sample was cooled to room temperature, and a spectrum was obtained. The spectra of adsorbed acrylamide and acrylic acid on TiO_2 also were obtained for comparison with the sample spectra. Acrylamide was adsorbed on TiO_2 by introducing the sample to its aqueous solution and then purging the solvent water with He for 1 h. Adsorption of acrylic acid was carried through the method described above for AN adsorption.

2.3. Characterization

The Brunauer–Emmett–Teller (BET) specific surface area of each sample was measured by N_2 adsorption under flow conditions (Nikkiso model 4232). X-ray powder diffraction (XRD) patterns were measured at 40 kV and 100 mA of X-ray power (Rigaku RU-300). Ag particle size was measured by means of transmission electron microscopy (TEM) using a Hitachi H-9000. Mean particle size was calculated from at least 100 Ag particles for Ag-ZSM-5, Ag/Al_2O_3, Ag/TiO_2, and Ag/SiO_2. For Ag/ZrO_2 and Ag/MgO, at least 15 Ag particles were used for calculation. The molar amount of exposed Ag was calculated from dispersion, estimated as dispersion = $1.34/d$ (nm) [18,24], where d is the mean particle size. Ultraviolet–visible (UV–vis) spectra were obtained under atmospheric conditions for fresh samples (Hitachi U-3500). $BaSO_4$ was used to obtain a background spectrum for each of the samples except for Ag/TiO_2; because TiO_2 absorbs strongly, TiO_2 powder calcined at 500 °C was used for the Ag/TiO_2 background. The sample used in AN decomposition also was measured. AN decomposition was carried out in a conventional flow reactor at 400 °C for 3 h, and then quenched with He flow. Temperature-programmed reduction by H_2 (H_2-TPR) was carried out with a temperature-programmed desorption (TPD) apparatus equipped with a TCD (Ohkura-Riken ADT700). Profiles from room temperature to 600 °C were obtained in a 100 ml/min flow of 2% H_2/Ar at a heating rate of 10 °C/min after pretreatment in a 5% O_2/He flow at 500 °C for 2 h. For comparison, a profile of Ag_2O (Wako, 99.9%) was measured. TPD of NH_3 (NH_3-TPD) was carried out with a TPD apparatus equipped with a mass spectrometer (Bel Japan TPD-1-AT). TPD profiles in the range of 100–500 °C were obtained in He at a flow rate of 50 ml/min and a heating rate of 10 °C/min after adsorption of NH_3 at 100 °C. TPD of CO_2 (CO_2-TPD) was carried out in the TPD apparatus used for the H_2-TPR tests. TPD profiles in the range of 100–500 °C were obtained in He at a flow rate of 50 ml/min and a heating rate of 10 °C/min after adsorption of CO_2 at 100 °C.

3. Results and discussion

3.1. AN decomposition activity

We previously reported the AN decomposition activity of various supported Ag catalysts [6]. Table 1 summarizes the AN de-

Table 1
Catalytic activity of supported Ag catalysts for AN decomposition.

Catalyst	T_{50} of AN conversion (°C)[a]	TOF at T_{50} (mmol/Ag-mol/s)	Maximum N_2 selectivity (%)[c]	TOF of N_2 at maximum selectivity (mmol/Ag-mol/s)
Ag-ZSM-5	433 (494)	0.86	55 (500)	0.49
Ag/Al_2O_3	383 (436)	7.8	52 (500)	3.3
Ag/TiO_2	281 (337)	4.7	87 (350)	1.9
Ag/SiO_2	274 (–[b])	16	84 (350)	6.6
Ag/ZrO_2	228 (311)	140	67 (300)	55
Ag/MgO	267 (490)	99	63 (300)	32

[a] The value in parenthesis is the activity of support.
[b] Negligible activity at whole temperatures measured.
[c] The value in parenthesis is temperature at which maximum N_2 selectivity was obtained.

composition activity. The temperature at which 50% AN conversion was observed (T_{50}) decreased in the order Ag-ZSM-5 > Ag/Al_2O_3 > Ag/TiO_2 > Ag/SiO_2 > Ag/MgO > Ag/ZrO_2. Ag/TiO_2 and Ag/SiO_2 exhibited the highest selectivity for N_2 at 350 °C. The N_2 selectivities of Ag/ZrO_2 and Ag/MgO both were approximately 65% at 300 °C, but the N_2 selectivities of Ag-ZSM-5 and Ag/Al_2O_3 never exceeded 55%.

T_{50} values for AN conversion over the support materials in the absence of Ag also are given in Table 1. Obviously, the addition of Ag enhanced AN conversion in all cases. For SiO_2, the addition of Ag resulted in the most substantial decrease in T_{50}, because SiO_2 had negligible activity for AN decomposition. MgO also exhibited a significant decrease in T_{50} on the addition of Ag. For ZrO_2, T_{50} decreased by approximately 80 °C. For ZSM-5, Al_2O_3, and TiO_2, T_{50} decreased by approximately 50–60 °C. We also calculated the turnover frequency (TOF) of both AN conversion and N_2 formation (Table 1). The values were calculated from the molar amounts of exposed Ag (Table 2). Ag/ZrO_2 and Ag/MgO showed significantly higher TOF values than the other catalysts. These results suggest that Ag species on SiO_2, ZrO_2, and MgO had very high reaction rates of AN decomposition.

Fig. 1 shows product selectivity at 400 °C. Ag/TiO_2 had the highest N_2 selectivity. Ag/SiO_2 also had >50% N_2 selectivity, as well as the highest N_2O selectivity. Ag/ZrO_2 and Ag/MgO formed small amounts of N_2 and large amounts of NO_x and N_2O. Less N_2 formation occurred with Ag-ZSM-5 and Ag/Al_2O_3 than with Ag/TiO_2 and Ag/SiO_2. Substantial amounts of nitrogen-containing byproducts were formed over Ag-ZSM-5 and Ag/Al_2O_3; HCN, HNCO, and CH_3CN were formed on Ag-ZSM-5, and mainly NH_3 was formed on Ag/Al_2O_3. These results suggest that Ag/TiO_2 exhibited the most preferable selectivity. Ag/SiO_2 also was favorable for AN decomposition. Notably, the main carbon-containing products formed in all of the experiments were CO_2 and, to a lesser extent, CO. With Ag-ZSM-5, small amounts of C_2H_4 and C_3H_6 were formed as well. No CH_4 or H_2 was observed in any of the cases. At temperatures below 400 °C, the nitrogen and carbon balance was >95% for all catalysts.

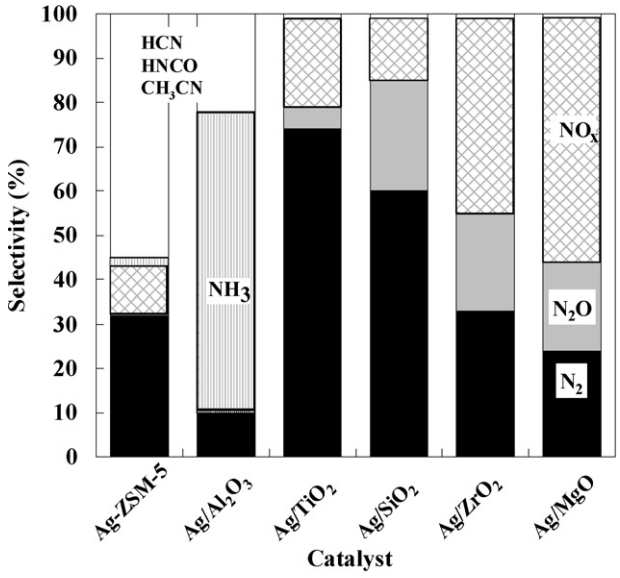

Fig. 1. Product selectivity in AN decomposition at 400 °C over Ag catalysts. The weight of each catalyst was 0.1 g, and the feed gas composition was ca. 200 ppm AN and 5% O_2 in He, with a total flow rate of 160 ml/min.

3.2. Characterization of the Ag species

Comparison of observed catalytic activities with the BET surface areas of the catalysts (Table 2) reveals no correlation between these two parameters. The mean particle size of Ag for each catalyst was measured from TEM images (Table 2). Ag was highly dispersed on ZSM-5 and TiO_2. The mean particle size of Ag was larger on Al_2O_3 than on ZSM-5 and TiO_2. Notably, Al_2O_3 had a wide distribution of particle sizes from 5 to 100 nm, with a mode value in particle size distribution of 10–20 nm. Ag particles on SiO_2 were of medium size, whereas Ag particles on ZrO_2 and MgO were very large (Table 2).

Fig. 2 shows the XRD profiles of the Ag catalysts. It shows no peaks that can be ascribed to metallic Ag or Ag_2O in the Ag-ZSM-5

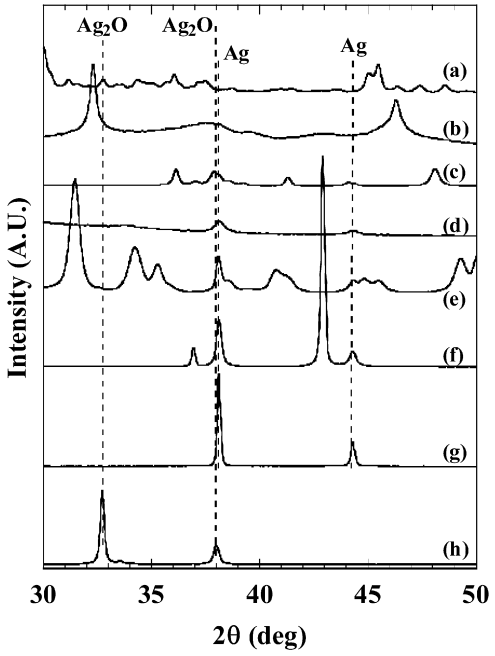

Fig. 2. XRD profiles for supported Ag catalysts: (a) Ag-ZSM-5, (b) Ag/Al_2O_3, (c) Ag/TiO_2, (d) Ag/SiO_2, (e) Ag/ZrO_2, (f) Ag/MgO, (g) Ag, and (h) Ag_2O.

Table 2
Characteristics of Ag catalysts.

Catalyst	BET surface area (m^2/g)	Mean particle size (nm)[a]	Exposed Ag (μmol/g)[b]	H_2 cons. (μmol/g)	H/Ag ratio[c]	Ag species				
						Ag	Ag_n	$Ag_n^{\delta+}$	Ag^+	Ag_2O
Ag-ZSM-5	259	4.3	142	350	1.02		○	○	○	
Ag/Al_2O_3	172	33	18	145	0.62		○	○	○	○
Ag/TiO_2	36	11	56	55	0.24	○	○			○
Ag/SiO_2	455	38	16	60	0.26	○			○	
Ag/ZrO_2	38	340	1.8	7	0.03	○				
Ag/MgO	13	250	2.5	5	0.02	○				

[a] Particle size was measured from TEM images.
[b] Calculated from mean particle size.
[c] The value was calculated from H_2 consumption determined by H_2-TPR; a value of unity indicates stoichiometric reduction of Ag_2O.

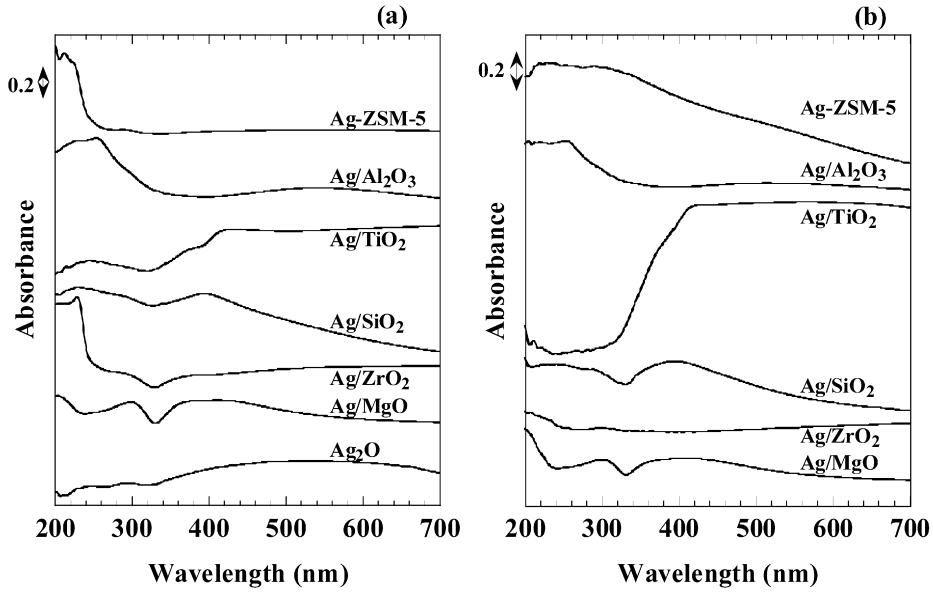

Fig. 3. UV–vis spectra for (a) Ag catalysts and (b) Ag catalysts used in AN decomposition. The weight of each catalyst was 0.1 g, the feed gas composition was ca. 200 ppm AN and 5% O_2 in He, with a total flow rate of 160 ml/min, and the reaction temperature was 400 °C.

and Ag/Al_2O_3 profiles. The lack of a diffraction peak in Ag-ZSM-5 was due to high dispersion of the Ag particles, as suggested by the mean particle size observed for this sample (Table 2). But Ag/Al_2O_3 also did not exhibit a diffraction peak, although its mean particle size was relatively large; this observation is explained in greater detail below. The Ag/TiO_2, Ag/SiO_2, Ag/ZrO_2, and Ag/MgO profiles all contained peaks characteristic of metallic Ag. The Ag particle size for Ag/TiO_2 could not be estimated, owing to superposition of the Ag and TiO_2 (anatase) peaks, but the lack of clear metallic peaks in the Ag/TiO_2 XRD profile suggests that the particles were smaller than those on MgO, ZrO_2, and SiO_2.

In the UV–vis spectra (Fig. 3a), Ag_2O exhibited a very broad band above 330 nm. Ag-ZSM-5 displayed absorption bands at 210, 225, and 265–310 nm. We attributed the bands at 210 and 225 nm to the $4d^{10}$–$4d^9 5s^1$ transition of isolated Ag^+ ions [19,20], and the small band at 265–310 nm was attributed to oligomeric Ag_n clusters [21]. Ag/Al_2O_3 exhibited absorption bands at 220, 250, 280–300, and 420–700 nm. The band at 220 nm was attributed to Ag^+ ions, the band at 250 nm was attributed to partly cationic Ag clusters ($Ag_n^{\delta+}$) [22,23], and the bands at 280–300 nm were attributed to Ag_n clusters [13]. The bands at 420–700 nm were attributed to Ag_2O. Ag/TiO_2 exhibited absorption bands at 250 and 370 nm. These bands were assigned to $Ag_n^{\delta+}$ and Ag_n clusters, respectively [23,24]. Ag/SiO_2 exhibited absorption bands at 230, 290, and 400 nm. We attributed the former two bands to Ag^+ and metallic Ag, respectively, and the latter band to the plasmon resonance of Ag aggregates [22,25]. Ag/ZrO_2 showed bands at 270–290 nm, which were attributed to metallic Ag. We confirmed that a band at 225 nm also was observed for ZrO_2. Ag/MgO had absorption bands at 290 and 380 nm, which were attributed to metallic Ag and the plasmon resonance of Ag aggregates, respectively.

To confirm that Ag species maintained their oxidation states during AN decomposition, UV–vis spectra were acquired for the samples used in AN decomposition (Fig. 3b). The spectra of Ag/SiO_2 and Ag/MgO after AN decomposition were nearly identical to those obtained for the unused catalysts. For Ag/Al_2O_3, the bands at 420–700 nm decreased slightly. This suggests that the composition of the Ag species in the fresh samples was retained in AN decomposition. For Ag/ZSM-5, the absorption at 240–360 nm increased in the spectrum of the sample used in AN decomposition, suggesting that some Ag^+ ions changed into $Ag_n^{\delta+}$ and Ag_n during AN decomposition. For Ag/TiO_2, the band at 250 nm diminished, suggesting that $Ag_n^{\delta+}$ disappeared during AN decomposition. For Ag/ZrO_2, the band at 225 nm due to ZrO_2 decreased, and no change in Ag species absorption was observed.

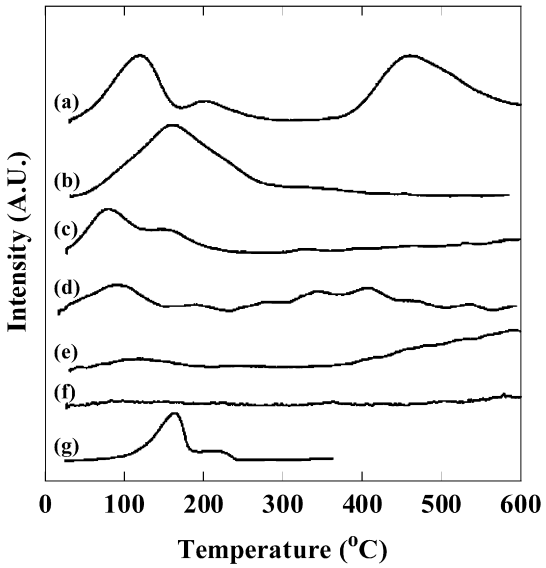

Fig. 4. H_2-TPR profiles for Ag catalysts: (a) Ag-ZSM-5, (b) Ag/Al_2O_3, (c) Ag/TiO_2, (d) Ag/SiO_2, (e) Ag/ZrO_2, (f) Ag/MgO, and (g) Ag_2O.

In the H_2-TPR profiles (Fig. 4), Ag/ZrO_2 and Ag/MgO had no distinct H_2 consumption peaks. In contrast, the Ag/SiO_2 profile exhibited several peaks, with the peak near 90 °C the strongest. The Ag/TiO_2 profile had a peak at 80 °C and a shoulder at 160 °C, and the Ag/Al_2O_3 profile also had a broad peak at 160 °C. The Ag-ZSM-5 profile had three peaks at 120, 220, and 460 °C. The reduction of Ag_2O occurred at 160 °C, as shown in profile (g) in Fig. 4. Therefore, we attributed the peaks for Ag/TiO_2 and Ag/Al_2O_3 observed near 160 °C to the reduction of Ag_2O. The lack of a band attributed to Ag_2O in UV–vis spectrum of Ag/TiO_2 was probably due to the small amount of Ag_2O. Considering the UV–vis spectra, we attributed the peak at 90 °C in the Ag/SiO_2 profile to the reduction of highly dispersed Ag^+. In addition, the peak at 80 °C

Table 3
NH_3 and CO_2 uptake of support materials.

Support	NH_3 uptake (μmol/g)	NH_3 uptake (μmol/m^2)	CO_2 uptake (μmol/g)	CO_2 uptake (μmol/m^2)
ZSM-5	460	1.2	0	0
Al_2O_3	48	0.3	15	0.1
TiO_2	24	0.4	2.9	0
SiO_2	1.8	0	0	0
ZrO_2	15	0.4	44	1
MgO	0.3	0	79	7.9

in the Ag/TiO_2 profile might be attributed to dispersed $Ag_n^{\delta+}$. For Ag-ZSM-5, we attributed the peaks at 120 and 460 °C to the reduction of Ag^+ ions and $Ag_n^{\delta+}$ formed by Ag^+ reduction, respectively, because Shibata et al. reported that the reduction of Ag^+ proceeds stepwise through an oxidized Ag cluster [26].

Values for the ratio of the amount of H consumption to the amount of Ag are given in Table 2. Here, using the stoichiometry of the reduction of Ag_2O ($Ag_2O + H_2 \rightarrow 2Ag + H_2O$) as a standard, a value of unity indicates that the amount of H_2 consumed was equivalent to the amount of Ag_2O reduced. As summarized in Table 2, the consumption of H_2 was almost stoichiometrically equivalent to the amount of Ag present in Ag-ZSM-5. In contrast, the ratios for the other catalysts were less than unity and were quite small for Ag/ZrO_2 and Ag/MgO in particular. These results suggest that the Ag particles were mostly metallic on ZrO_2 and MgO, were partially oxidized on TiO_2 and SiO_2, and were highly oxidized on ZSM-5 and Al_2O_3. Considering these results for Ag/Al_2O_3, a possible reason for the lack of diffraction peak in the XRD profile of Ag/Al_2O_3, regardless of the sample's relatively large particle size, might be that both metallic and oxidized Ag species coexisted in each particles. Table 2 summarizes the Ag species that were likely present on each of the supports during AN decomposition, on the basis of all of the characterization results for the Ag catalysts.

3.3. Correlation of Ag oxidation states with support material characteristics

Table 3 lists the NH_3 and CO_2 uptake values estimated from NH_3- and CO_2-TPD of the support materials. The amount of acidic sites (NH_3 uptake per unit weight) decreased in the order ZSM-5 > Al_2O_3 > TiO_2 > ZrO_2 > SiO_2 > MgO, and the amount of basic sites (CO_2 uptake per unit weight) decreased in the order MgO > ZrO_2 > Al_2O_3 > TiO_2 > SiO_2 ∼ ZSM-5. NH_3 uptake exceeded CO_2 uptake for ZSM-5, Al_2O_3, and TiO_2, whereas CO_2 uptake exceeded NH_3 uptake for ZrO_2 and MgO. Adsorption of both NH_3 and CO_2 was negligible for SiO_2. These results suggest that the surfaces of ZSM-5, Al_2O_3, and TiO_2 were acidic; the surface of SiO_2 was neutral; and the surfaces of ZrO_2 and MgO were basic. Because Ag_2O reacts with CO_2 to form Ag_2CO_3 [27], Ag_2O should have some basic character. Considering the Ag species present on each support (Table 2) along with the basicity of Ag_2O, we suspect that the acidic supports, ZSM-5 and Al_2O_3, favored the formation of highly dispersed, oxidized Ag species. In contrast, the basic supports ZrO_2 and MgO should have favored the formation of metallic Ag particles. We also suspect that the neutral support, SiO_2, formed mostly metallic Ag particles with a small amount of Ag oxide, whereas weakly acidic TiO_2 formed both oxidized and metallic Ag. Thus, we concluded that the acid–base characteristics of the support surface influenced the oxidation state of the Ag deposited on the supports.

3.4. Correlation between Ag species and AN decomposition activity

The oxidized Ag species on the acidic ZSM-5 and Al_2O_3 supports exhibited low TOF and high T_{50} values, whereas the metallic Ag present on the TiO_2, SiO_2, ZrO_2, and MgO supports exhibited low T_{50} values and high N_2 selectivities (Table 1). These results suggest that metallic Ag was necessary for the formation of N_2 in the decomposition of AN. However, the presence of metallic Ag, which was found in large quantities on the basic ZrO_2 and MgO supports, also corresponded to substantial NO_x formation (Fig. 1). The oxidized Ag species on ZSM-5 and Al_2O_3 exhibited different selectivities for nitrogen-containing byproducts. The UV–vis and H_2-TPR results indicated that most of the Ag on ZSM-5 was dispersed as Ag^+ ions in the fresh sample, whereas $Ag_n^{\delta+}$ and Ag_n clusters appeared in the spent sample. The UV–vis and H_2-TPR results also indicated that the Ag species on Al_2O_3 consisted mainly of Ag_2O and clusters of $Ag_n^{\delta+}$ and Ag_n. Ag^+ ions, $Ag_n^{\delta+}$, and Ag_n clusters would be involved in the cleavage of C=C and C–C bonds to form HCN, HNCO, and CH_3CN, whereas the dispersed Ag_2O would be involved in NH_3 formation. Our results suggest that each Ag species had a different catalytic activity for AN decomposition.

3.5. Effect of the coexistence of metallic and oxidized Ag

To examine the effect of coexistence of metallic and oxidized Ag species (as was the case for Ag/TiO_2 and Ag/SiO_2), we carried out TPSR of AN under a flow of 1% O_2/He for oxidized and reduced Ag/TiO_2, as well as for the bare TiO_2 support (Fig. 5). The oxidized Ag/TiO_2 exhibited AN desorption at around 130 °C, whereas the reduced Ag/TiO_2 showed only a small amount of AN desorption at low temperatures. The AN uptake values estimated from the total amount of evolved carbon for oxidized and reduced Ag/TiO_2 and TiO_2 were 0.16, 0.11, and 0.13 mmol/g, respectively, and the corresponding percentages of unreacted AN that desorbed from the sample were 49%, 18%, and 29%. Because the reduced Ag/TiO_2 is expected to contain the largest amount of metallic Ag of the samples tested, these results suggest that metallic Ag promoted AN conversion.

More NO_x was formed over reduced Ag/TiO_2 than over oxidized Ag/TiO_2 (Fig. 5). The NO_x selectivities for oxidized and reduced Ag/TiO_2 were 3% and 21%, respectively. These results agree with the results indicating that Ag/ZrO_2 and Ag/MgO (Fig. 1), which contained large proportions of metallic Ag, showed high NO_x formation. Furthermore, the temperature of CO_2 formation over the reduced Ag/TiO_2 was lower than that over the oxidized Ag/TiO_2. Notably, H_2O was formed at almost the same peak temperature as that observed for CO_2 and CO formation. Metallic Ag clearly exhibited greater oxidizing ability, in agreement with previous reports [22,28].

For all catalysts, NH_3 was formed first in the TPSR measurements. The peak temperatures for NH_3 formation were 140 °C for oxidized Ag/TiO_2, 180 °C for reduced Ag/TiO_2, and 185 °C for TiO_2. The fact that the peak temperature for the reduced Ag/TiO_2 was in good agreement with that for the bare TiO_2 support suggests that NH_3 was formed on bare TiO_2. The shift of the peak toward lower temperatures for the oxidized Ag/TiO_2 catalyst indicates that the oxidized Ag species further enhanced the formation of NH_3 on TiO_2.

3.6. Possible reaction pathway for the decomposition of AN

To clarify a formation pathway of NH_3, which was the first product observed in TPSR, DRIFTS spectra were acquired during TPSR over TiO_2, under the same gaseous conditions as used to acquire the data in Fig. 5. The results are shown in Fig. 6a. After AN adsorption at room temperature, bands appeared at 2294, 2262, and 2235 cm^{-1}, which were attributed to the C≡N functional group in AN [29–31]. These bands decreased with increasing temperature and disappeared at 150 °C. During TPSR, NH_3 was formed above 100 °C, resulting in the conversion of a portion of the C≡N to NH_3. Moreover, no carbon-containing products were observed in

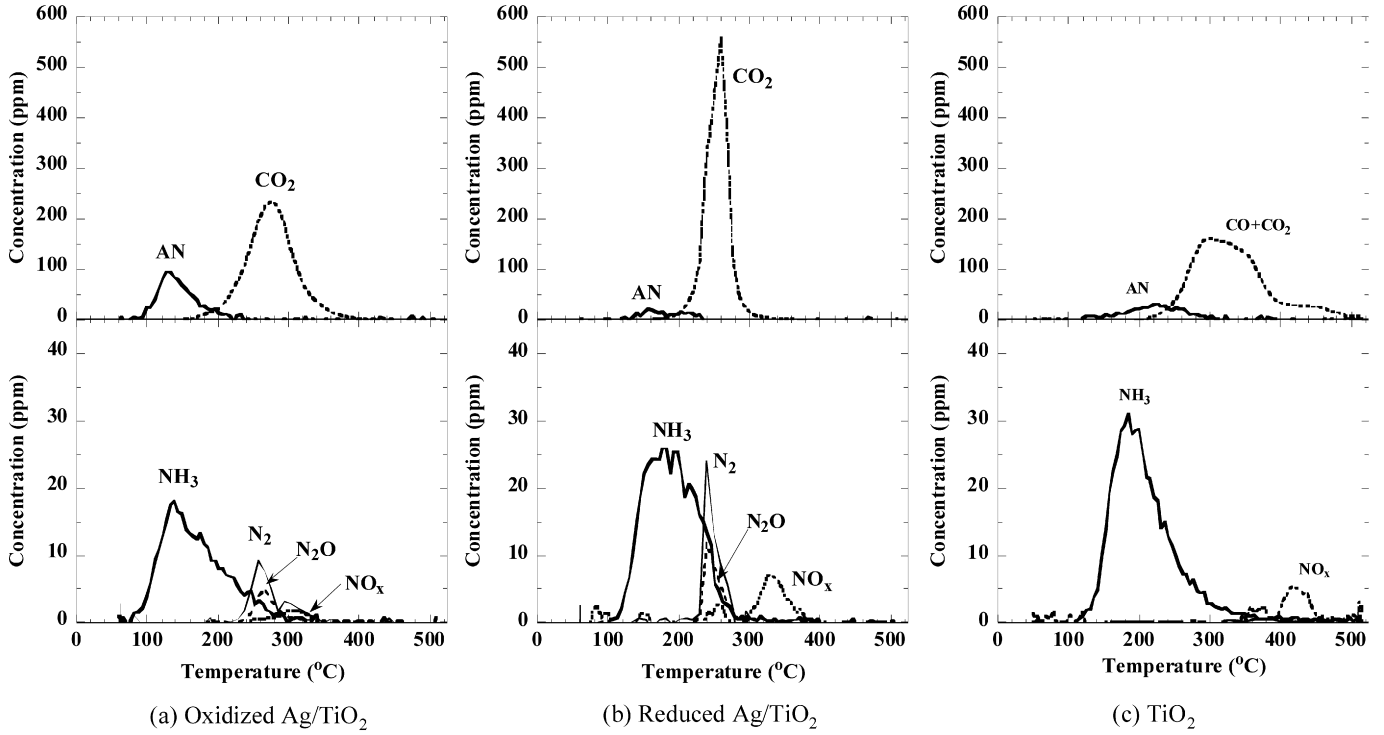

Fig. 5. TPSR profiles for the oxidized (a) and reduced Ag/TiO_2 (b) and for the bare TiO_2 support (c). The weight of each sample was 0.1 g. The AN adsorption temperature was 50 °C. TPSR was carried out in 1% O_2/He at a flow rate of 160 ml/min.

the TPSR profiles below 150 °C, suggesting that all of the carbon in AN was retained on the TiO_2 surface. Bands at 1700–1350 cm^{-1} were observed in the DRIFTS spectra, and these bands increased in intensity up to 200 °C; we believe that these bands should be assigned to carbon-containing adsorbed species. Above 150 °C, additional bands appeared at 3417, 3371, and 3276 cm^{-1}, ascribed to adsorbed NH_x ($1 < x < 3$) [32].

A possible pathway for the formation of NH_3 from AN is hydrolysis. Hydrolysis of AN proceeds through the following sequential reactions:

$$CH_2{=}CH{-}C{\equiv}N + H_2O \rightarrow CH_2{=}CH{-}CONH_2 \quad \text{(acrylamide)},$$

$$CH_2{=}CH{-}CO{-}NH_2 + H_2O \rightarrow NH_3 + CH_2{=}CH{-}COOH \quad \text{(acrylic acid)}.$$

To confirm whether NH_3 was formed through hydrolysis, we compared the changes in the DRIFTS spectral bands at around 1700–1500 cm^{-1} with the changes in the spectral bands in TPSR of acrylamide adsorbed on TiO_2. In TPSR of AN, the bands at 1662 and 1560 cm^{-1} decreased with increasing temperature; in contrast, the bands at 1637, 1521, and 1442 cm^{-1} increased with increasing temperature. In the case of TPSR of acrylamide, the adsorbed acrylamide at room temperature exhibited bands at 1676, 1591, 1436, and 1364 cm^{-1} (Fig. 6b). The band at 1676 cm^{-1} decreased and shifted to 1662 cm^{-1} with increasing temperature. An additional band appeared at 1637 cm^{-1} at 100 °C. The band at 1591 cm^{-1} decreased and the band at 1521 cm^{-1} increased with increasing temperature. The band at 1436 cm^{-1} shifted to 1445 cm^{-1} and increased with increasing temperature. The bands appearing with increasing temperature were identical to those observed for acrylic acid adsorbed on TiO_2. The changes in the bands at 1662, 1637, 1560, 1521, and 1442 cm^{-1} observed during TPSR of AN were in agreement with the changes in the bands observed during TPSR of acrylamide. The bands at 1560, 1521, and 1442 cm^{-1} observed during TPSR of AN were attributed to overlapping bands of acrylamide and acrylic acid. Therefore, the formation of NH_3 at low temperature during TPSR of AN was suspected to proceed through AN hydrolysis.

We carried out the same DRIFTS measurements with oxidized and reduced Ag/TiO_2; the results are shown in Fig. 7. For oxidized Ag/TiO_2, the DRIFT spectral bands at 2262 and 2235 cm^{-1} attributed to AN were weak even at room temperature (Fig. 7a). A band at 1542 cm^{-1}, likely due to overlapping of the bands at 1560 and 1521 cm^{-1}, appeared at all temperatures. The bands at 1442 and 1369 cm^{-1}, which were assigned to acrylic acid, also were observed even at room temperature. An additional band appeared at 1350 cm^{-1} above 50 °C, which was assigned to a species of formate [33,34]. Because metallic Ag remained after the oxidizing pretreatment, as evidenced by the H_2-TPR data, the formate species might have been formed by subsequent oxidation of acrylic acid on this metallic Ag. NH_x ($1 < x < 3$) bands appeared at 3407, 3350, and 3255 cm^{-1} and were slightly shifted toward lower wavenumbers compared with the corresponding bands observed for bare TiO_2, even at room temperature. The band observed at 3467 cm^{-1} was assigned to NH_x species [35]. These spectra suggest that hydrolysis-induced derivatives of AN adsorbed on oxidized Ag/TiO_2 were present even at room temperature; in other words, the oxidized Ag species strongly promoted AN hydrolysis. In the TPSR profiles, the apparent amount of AN desorption observed for oxidized Ag/TiO_2 exceeded the amounts observed for TiO_2 and reduced Ag/TiO_2, although the amount of molecularly adsorbed AN on oxidized Ag/TiO_2 was very small according to the DRIFTS spectra. A possible explanation for this discrepancy is the reversible desorption of AN from adsorbed AN derivatives on oxidized Ag/TiO_2.

We previously reported that AN decomposition over Cu-ZSM-5 proceeds by the hydrolysis of nitrogen-containing intermediates, such as –NCO [29]. No obvious –NCO bands were observed in the present case, however; thus, AN decomposition through the forma-

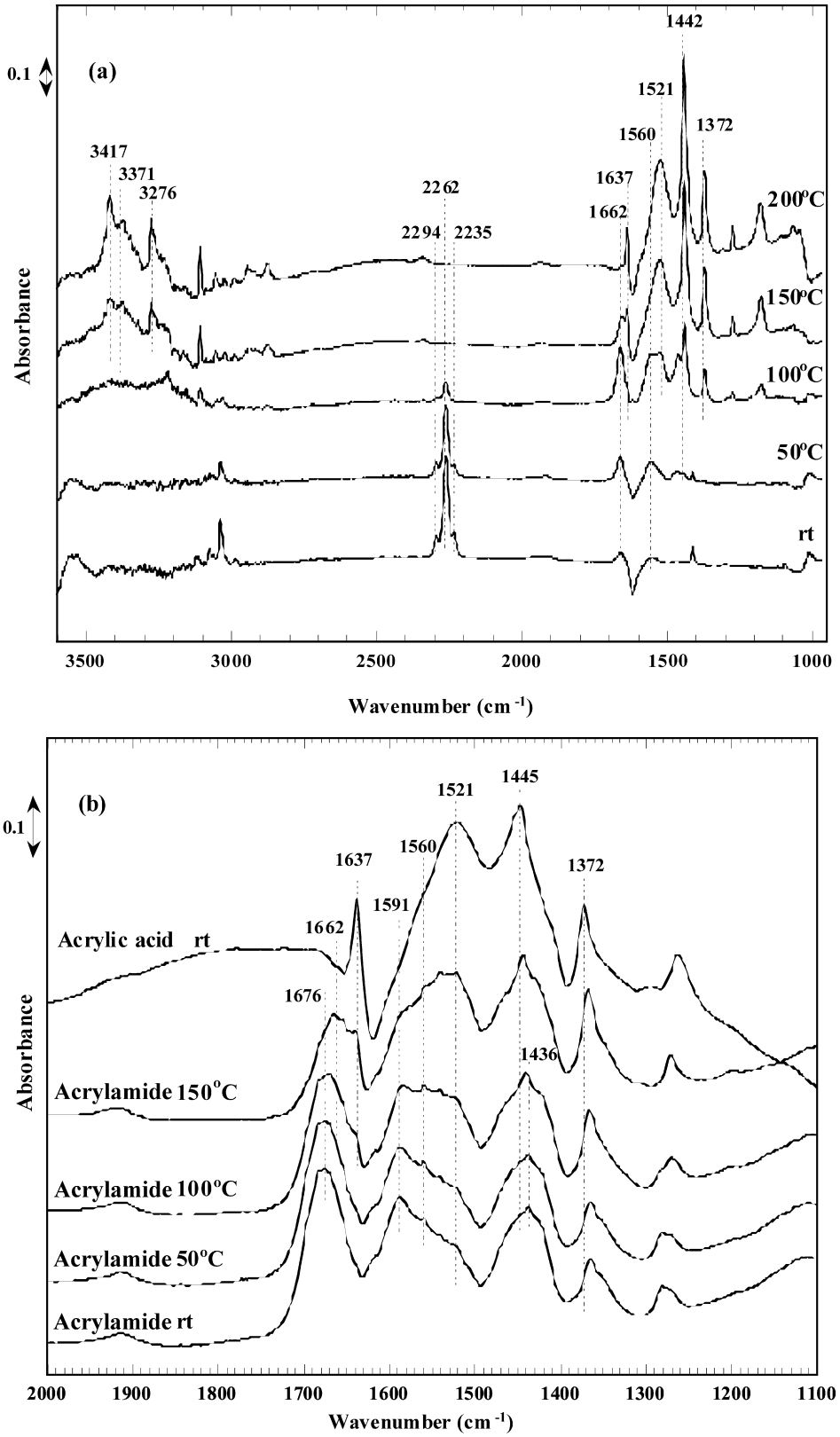

Fig. 6. In situ DRIFT spectra observed during TPSR of AN (a) and during TPSR of acrylamide (b) over TiO_2. The adsorption of AN, acrylamide, and acrylic acid was carried out at room temperature.

tion of –NCO and its hydrolysis to form NH_3 most likely does not proceed on the present Ag catalyst.

For reduced Ag/TiO_2, characteristic AN bands were observed in the region of 2300–2230 cm^{-1} at temperatures up to 100 °C (Fig. 7b). The changes in spectral features in this region with increasing temperature were similar to the trends observed over TiO_2. The TPSR measurements with reduced Ag/TiO_2 showed NH_3 formation, with peaks observed at the same temperature as those

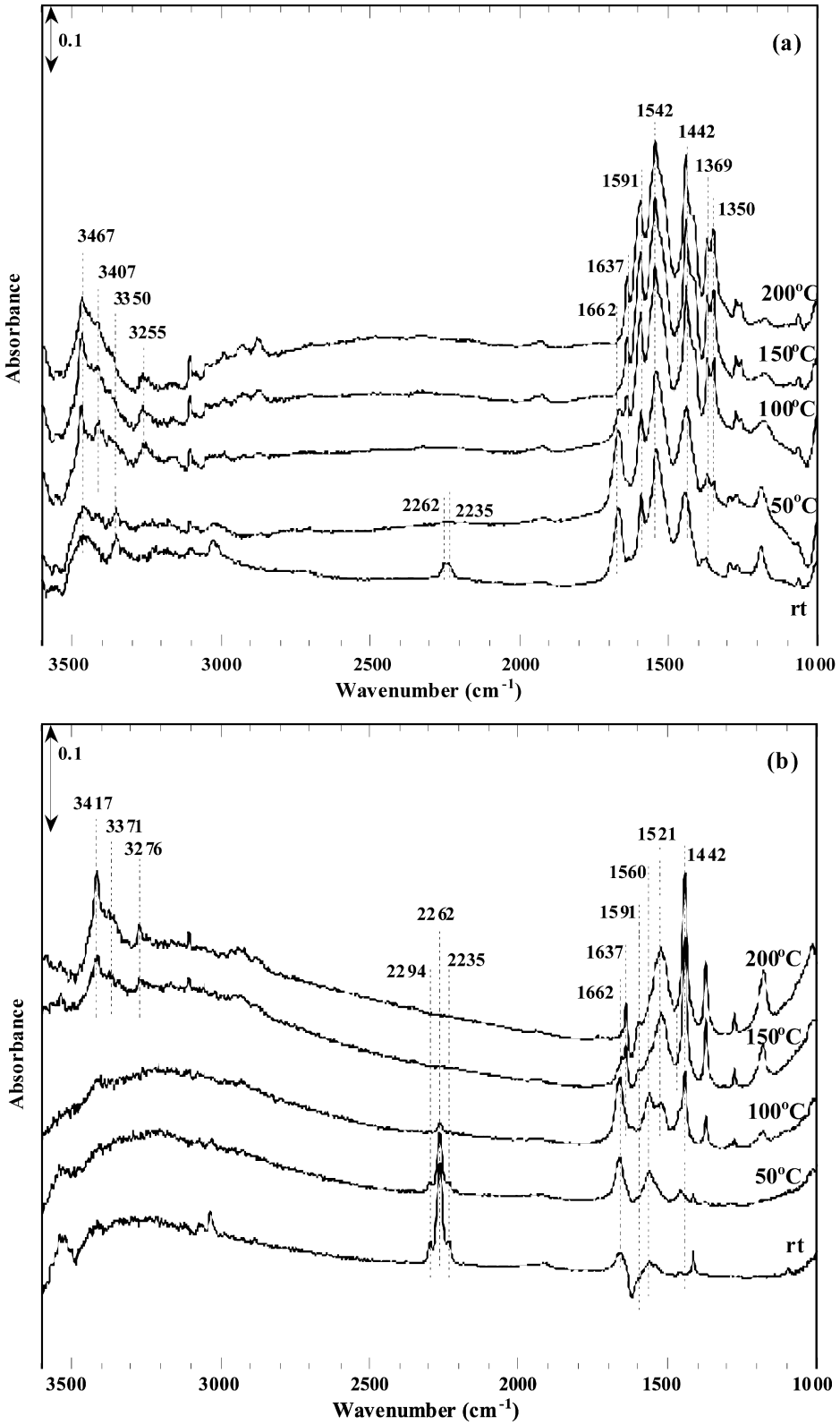

Fig. 7. In situ DRIFT spectra observed during TPSR of AN over oxidized Ag/TiO_2 (a) and reduced Ag/TiO_2 (b).

observed for TiO_2. The similarity of the trends in the DRIFTS spectra for the reduced Ag/TiO_2 and the bare TiO_2 support suggests that metallic Ag made only a small contribution to the reaction pathway of AN hydrolysis.

We previously reported that the selectivity of Ag/TiO_2 for N_2 in the decomposition of AN nearly coincides with its selectivity for NH_3 oxidation [6]. A speculated reaction pathway of AN decomposition to form N_2 over Ag/TiO_2 is the formation of NH_3 by hydrolysis of AN with subsequent oxidation of NH_3 to form N_2. Considering that the hydrolysis-induced derivatives of AN were formed in the absence of H_2O feed, AN should be hydrolyzed by surface hydroxyl groups. In the steady-state reaction, NH_3 formed

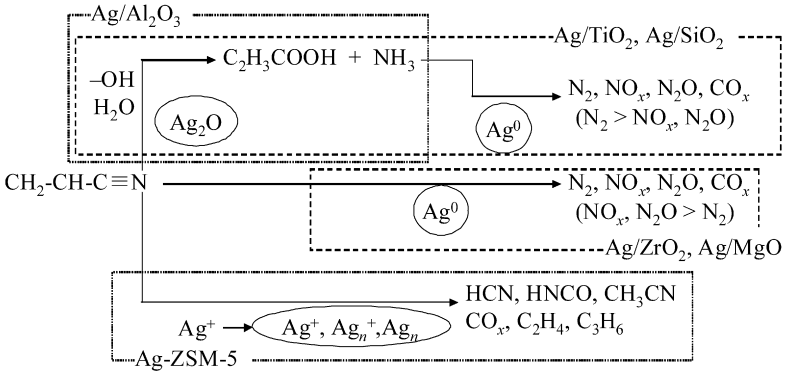

Fig. 8. Speculated reaction pathway of AN decomposition over Ag catalysts.

from AN hydrolysis should be oxidized to form N_2 and H_2O. Therefore, the hydroxyl group consumed by AN hydrolysis was converted into H_2O, allowing regeneration of hydroxyl groups.

The speculated reaction pathway of AN hydrolysis over Ag catalysts is illustrated in Fig. 8. AN hydrolysis proceeded on oxidized Ag species, most likely Ag_2O. Intermediate NH_3 and acrylic acid were oxidized into N_2 and CO_x ($CO + CO_2$), respectively, over metallic Ag. The direct oxidation of AN over large metallic Ag particles in Ag/ZrO_2 and Ag/MgO formed large amounts of NO_x and N_2O. For Ag-ZSM-5, AN was decomposed into nitrogen-containing products and some hydrocarbons over Ag^+, $Ag_n^{\delta+}$, and Ag_n clusters.

The high activity of Ag/SiO_2, regardless of the inactivity of SiO_2, is due to a combination of AN hydrolysis and NH_3 oxidation by oxidized and metallic Ag, respectively. Therefore, Ag/SiO_2 should have activities for AN decomposition similar to those of Ag/TiO_2. In our previous work, we reported that AN conversion and N_2 selectivity over Ag/TiO_2 were enhanced by the addition of H_2O to the feed gas. The TOF for N_2 formation became 1.4 times higher at 300 °C when H_2O was added. Conversion of AN and formation of NH_3 over Ag/SiO_2 also were increased by the addition of H_2O [6]. Although the addition of H_2O should enhance the rate of AN hydrolysis on oxidized Ag species, NH_3 should be easily released from the catalyst surface without interacting with the SiO_2 support. The presence of NH_3 adsorption sites on the support material would promote the retention of NH_3, which might then be converted to N_2.

For Ag-ZSM-5 and Ag/Al_2O_3, oxidized Ag species, such as Ag^+, $Ag_n^{\delta+}$, and Ag_2O, accounted for most of the Ag species; thus, the oxidation ability of this catalyst should be lower than that of the other catalysts. The low oxidative capacity of Ag-ZSM-5 and Ag/Al_2O_3 due to the absence or deficiency of metallic Ag not only decreased N_2 formation, but also may have decreased AN conversion. We have previously reported that acrylic acid formed from the hydrolysis of AN can easily lead to a carbonaceous deposit on acidic zeolite [36]. The low oxidation ability observed for Ag-ZSM-5 and Ag/Al_2O_3 might result from the covering of this surface by accumulated carbonaceous deposits.

Our results indicate that the best supports for the decomposition of AN were those containing both metallic and oxidized Ag species, as well as NH_3 adsorption sites. We conclude that the high AN decomposition activity and N_2 selectivity of Ag/TiO_2 resulted from AN hydrolysis to form NH_3 over the oxidized Ag species and subsequent NH_3 oxidation over metallic Ag.

4. Conclusion

We studied the effect of the support material on the Ag-catalyzed decomposition of AN, in which AN was converted to CO_2, H_2O, and N_2. The conversion of AN increased in the order Ag-ZSM-5 < Ag/Al_2O_3 < Ag/TiO_2 < Ag/SiO_2 < Ag/MgO < Ag/ZrO_2. Ag/TiO_2 and Ag/SiO_2 exhibited high N_2 selectivities (>80%) at 350 °C. Although Ag/ZrO_2 and Ag/MgO exhibited high AN decomposition activities, substantial amounts of NO_x were formed. With Ag-ZSM-5 and Ag/Al_2O_3, substantial amounts of nitrogen-containing products were formed, including HCN, HNCO, CH_3CN, and NH_3. Comparing the activities of the Ag-containing catalysts with those of the support materials alone indicates that Ag substantially enhanced the decomposition of AN on TiO_2, ZrO_2, SiO_2, and MgO. XRD, UV–vis, and H_2-TPR results indicate that the Ag species on ZSM-5 and Al_2O_3 were mainly Ag oxides, including Ag_2O, Ag^+ ions, and $Ag_n^{\delta+}$; that those on TiO_2 and SiO_2 were both metallic and oxidized species; and that those on ZrO_2 and MgO were mostly in the metallic state. Our results suggest that metallic Ag was necessary for the decomposition of AN to form N_2. NH_3- and CO_2-TPD were carried out to characterize the acid–base properties of the support material surfaces. The results suggest that the amount of metallic Ag present in the catalysts increased with increasing basicity of the support surface. TPSR of AN revealed that oxidized Ag/TiO_2 exhibited lower NO_x formation than reduced Ag/TiO_2 and that the oxidized catalyst promoted the formation of NH_3. DRIFTS spectra revealed that AN likely was hydrolyzed to acrylamide and acrylic acid. The oxidized Ag species promoted AN hydrolysis, and TiO_2 also hydrolyzed AN. We conclude that the high AN decomposition activity with high N_2 selectivity of Ag/TiO_2 and Ag/SiO_2 was due to the coexistence of oxidized and metallic Ag, which enabled AN hydrolysis and subsequent NH_3 oxidation, respectively.

References

[1] C. Jia, S. Batterman, C. Godwin, Atom. Environ. 42 (2008) 2083.
[2] D.R. van der Vaart, W.M. Vatvuk, A.H. Wehe, J. Air Waste Manage. Assoc. 41 (1991) 92.
[3] P. Papaefthimiou, T. Ioannides, X.E. Verykios, Appl. Catal. B 13 (1997) 175.
[4] H. Einaga, S. Futamura, J. Catal. 227 (2004) 304.
[5] H. Kim, S.M. Oh, A. Ogata, S. Futamura, Appl. Catal. B 56 (2005) 213.
[6] T. Nanba, S. Masukawa, J. Uchisawa, A. Obuchi, Catal. Lett. 93 (2004) 195.
[7] A. Gervasini, V. Ragaini, Catal. Today 60 (2000) 129.
[8] S.P. Felter, J.S. Dollarhide, Regul. Toxicol. Pharm. 26 (1997) 281.
[9] V. Muzyka, S. Veimer, N. Schmidt, Sci. Total Environ. 217 (1998) 103.
[10] W.-C. Hung, H. Chu, J. Environ. Eng. 132 (2006) 1482.
[11] S. Satokawa, Chem. Lett. (2000) 294.
[12] R. Burch, J.P. Breen, C.J. Hill, B. Krutzsch, B. Konrad, E. Jobson, L. Cider, K. Eränen, F. Klingstedt, L.-E. Lindfors, Top. Catal. 30–31 (2004) 19.
[13] K. Shimizu, J. Shibata, H. Yoshida, A. Satsuma, T. Hattori, Appl. Catal. B 30 (2001) 151.
[14] L. Gang, B.G. Anderson, J. van Grondelle, R.A. van Santen, Appl. Catal. B 40 (2003) 101.
[15] T. Miyadera, Appl. Catal. B 2 (1993) 199.
[16] T. Nakatsuji, R. Yasukawa, K. Tabata, K. Ueda, M. Niwa, Appl. Catal. B 17 (1998) 333.
[17] T. Nanba, A. Obuchi, Y. Sugiura, C. Kouno, J. Uchisawa, S. Kushiyama, J. Catal. 211 (2002) 53.
[18] J.K. Plischke, M.A. Vannice, Appl. Catal. 42 (1988) 255.
[19] C. Shi, M. Cheng, Z. Qu, X. Bao, Appl. Catal. B 51 (2004) 171.
[20] M. Matsuoka, W.-S. Ju, M. Anpo, Chem. Lett. (2000) 626.

[21] Z. Li, M. Flyszani-Stephanopoulos, J. Catal. 182 (1999) 313.
[22] K.A. Bethke, H.H. Kung, J. Catal. 172 (1997) 93.
[23] K. Sato, T. Yoshinari, Y. Kintaichi, M. Haneda, H. Hamada, Appl. Catal. B 44 (2003) 67.
[24] J. Lu, J.J. Bravo-Suárez, A. Takahashi, M. Haruta, S.T. Oyama, J. Catal. 232 (2005) 85.
[25] K.L. Kelly, E. Coronado, L.L. Zhao, G.C. Schatz, J. Phys. Chem. B 107 (2003) 668.
[26] J. Shibata, K. Shimizu, Y. Takada, A. Shichi, H. Yoshida, S. Satokawa, A. Satsuma, T. Hattori, J. Catal. 227 (2004) 367.
[27] W.S. Epling, G.B. Hoflund, G.N. Salaita, J. Phys. Chem. B 102 (1998) 2263.
[28] I.H. Son, M.C. Kim, H.L. Koh, K.L. Kim, Catal. Lett. 75 (2001) 191.
[29] T. Nanba, S. Masukawa, J. Uchisawa, A. Obuchi, J. Mol. Catal. A 276 (2007) 130.
[30] F. Poignant, J.L. Freysz, M. Daturi, J. Saussey, Catal. Today 70 (2001) 197.
[31] P.J. Chong, G. Curthoys, J. Chem. Soc. Faraday Trans. 1 77 (1981) 1649.
[32] N. Fripiat, M.-A. Centeno, P. Grange, Chem. Mater. 11 (1999) 1434.
[33] J.M. Pigos, C.J. Brooks, G. Jacobs, B.H. Davis, Appl. Catal. A 319 (2007) 47.
[34] M. Haneda, E. Joubert, J.-C. Ménézo, D. Duprez, J. Barbier, N. Bion, M. Daturi, J. Saussey, J.-C. Lavalley, H. Hamada, Phys. Chem. Chem. Phys. 3 (2001) 1371.
[35] D.Yu. Zemlyanov, M.Yu. Smirnov, V.V. Gorodetskii, Surf. Sci. 391 (1997) 37.
[36] T. Nanba, S. Masukawa, J. Uchisawa, A. Obuchi, Chem. Lett. 33 (2004) 924.